Topological and spectroscopic study of three-electron bonded compounds as models of radical cations of methionine-containing dipeptides

ARTICLE *in* CHEMICAL PHYSICS LETTERS · DECEMBER 2008

Impact Factor: 1.9 · DOI: 10.1016/j.cplett.2008.11.012

4 AUTHORS, INCLUDING:

Isabelle Fourré
Sorbonne universités, UPMC - Paris 6
16 PUBLICATIONS **274** CITATIONS
SEE PROFILE

Benoît Braïda
Pierre and Marie Curie University - Paris 6
47 PUBLICATIONS **693** CITATIONS
SEE PROFILE

Chantal Houée-Levin
Université Paris-Sud 11
125 PUBLICATIONS **1,560** CITATIONS
SEE PROFILE

Chemical Physics Letters 467 (2008) 164–169

Contents lists available at ScienceDirect

Chemical Physics Letters

journal homepage: www.elsevier.com/locate/cplett

Topological and spectroscopic study of three-electron bonded compounds as models of radical cations of methionine-containing dipeptides

Isabelle Fourré [a,*], Jacqueline Bergès [a,1], Benoît Braïda [a], Chantal Houée-Levin [b]

[a] Laboratoire de Chimie Théorique, UMR 7616, Université Pierre et Marie Curie, 4 Place Jussieu, 75252 Paris Cedex 5, France
[b] Laboratoire de Chimie Physique, UMR 8000, Université Paris Sud, F-91405 Orsay, France

ARTICLE INFO

Article history:
Received 1 August 2008
In final form 4 November 2008
Available online 8 November 2008

ABSTRACT

Small models of radical cations of methionine-containing dipeptides, which are stabilized by formation of two-centre three-electron (2c–3e) S∴X bonds (X = S, N and O), were investigated at the BH&HLYP/6-31G(d) level and by means of topological tools. The SX distance is not so important for stability but the relative orientation of both fragments is. The AIM and ELF topological analyses shows that the nature of the S∴X bond varies with X, from purely 2c–3e in S∴S$^+$ entities to electrostatic in S∴O$^+$ ones. The $\sigma_{SX} \rightarrow \sigma^*_{SX}$ wavelengths, obtained at the TD-BH&HLYP/cc-pVTZ level, strongly depend on X and on conformation.

1. Introduction

Methionine (Met) is an essential amino acid that should be provided by food. The redox reactions of Met or of its derivatives due to its thioether function are important in the cellular life. The sulphur function is susceptible to attack by oxygen or nitrogen free radicals in oxidative stress [1]. Met oxidation may be either a protection through its regeneration by enzyme systems [2] or a damaging event, associated to neurotoxicity of β amyloid peptide [3] and major cause for the functional impairment of actin filaments [4]. In oxidative stress, Met is first oxidized to its sulphur radical cation. Pulse radiolysis as well as flash photolysis data demonstrated that upon oxidation of a thioether function, the sulphur centred radical cation of very short lifetime (a few microseconds) underwent stabilization by complexation with the heteroatoms of the peptidic bond or a sulphur atom of another thioether group. It leads to so-called two-center three-electron (2c–3e) bonds [5], designated as S∴X, X = N, O or S (for review see [6,7] and references therein). Some interconversion between these radicals was observed: the (S∴O)$^+$-bonded intermediate can exist in an equilibrium with the intermolecularly S∴S-bonded radical cations.

Theoretical approaches concerned molecular modelling to examine the stability of the S∴X$^+$ bonds [8–12]. In their work on complexes between the radical cation of dimethylsulphide and models for several biologically available electron pair donors, Brunelle and Rauk [9] gave a description of the S∴X bond in terms of the commonly molecular orbital (MO) theory. In this description, the X atoms act by providing electron lone pairs that can stabilize sulphide radical cations (R2S$^{+\bullet}$) through the overlap of the heteroatoms' doubly occupied p orbitals with the singly occupied p orbital of the sulphur radical leading to a bonding σ_{SX} orbital and an antibonding σ^*_{SX} orbital. Another description is the Pauling's valence bond (VB) one [13], in which the (2c–3e) bond owes its stability to a resonance between two Lewis structures related by charge transfer as

$$S^{\bullet+}|X \leftrightarrow S|X^{\bullet+}$$

Our aim was to investigate the influence of the X atoms on structural and topological parameters of the S∴X bond in small radical models as well as on the associated $\sigma_{SX} \rightarrow \sigma^*_{SX}$ absorption wavelength. These models were chosen to explore the various S∴X bonds that can be formed in proteins, in which the S-containing amino acid methionine can be close either to another methionine residue, or to heteroatoms N or O coming from the peptidic group or from the N- or C-terminal group. For each representative model, we also tested the role of the relative positions of the two fragments on the 2c–3e bond. We used two different topological analyses that allow extraction of the chemical information from a local function: the electronic density in the atoms-in-molecules (AIM) method of Bader [14] or the electron localization function (ELF) of Becke and Edgecombe [15] in the topological description of the chemical bond developed by Silvi and Savin [16].

2. Methodology

2.1. Sketch of the ELF topological analysis

Since the method has already been detailed elsewhere [16,17] we will only recall its main features. The ELF topological analysis provides a partition of the molecular space into basins of attractors

* Corresponding author. Fax: +33 1 44 27 41 17.
E-mail addresses: fourre@lct.jussieu.fr (I. Fourré), jb@lct.jussieu.fr (J. Bergès), braida@lct.jussieu.fr (B. Braïda), chantal.houee@u-psud.fr (C. Houée-Levin).
[1] Also at Université Paris Descartes, 12, Rue de l'Ecole de Médecine, 75006 Paris, France.

0009-2614/$ - see front matter © 2008 Elsevier B.V. All rights reserved.
doi:10.1016/j.cplett.2008.11.012

Ω_i (the local maxima of ELF) which are of two kinds: the core basins noted C(X) which encompass the nuclei X with $Z > 2$, and the valence basins V(X,Y,...) (Y = another atom) which fill the remaining space. The valence basins are characterized by their synaptic order, i.e. the number of core basins with which they share a common separatrix. Monosynaptic basins V(X) correspond to conventional lone pairs, disynaptic basins V(X,Y) to two-center bonds, and polysynaptic basins to multicenter bonds. A quantitative model of the Lewis empirical theory is thus obtained. When dealing with radicals, of particular importance are the integrated basin spin densities

$$\langle S_z \rangle_{\Omega_i} = \frac{1}{2} \int_{\Omega_i} (\rho^{\alpha}(r) - \rho^{\beta}(r)) dr$$

where $\rho^{\sigma}(r)$ is the σ spin-one electron density distribution function.

2.2. Topological signatures of the 2c–3e bond

From our preceding works [18–20], four ELF topological signatures have been established for the 2c–3e X.·.Y bonding and are recalled in the Supplementary material.

In the AIM framework analysis, the partition of the molecular space leads to atomic basins only, thus the topological signatures reduce to three (see also the Supplementary material).

3. Computational details

Until now, the adequacy of theoretical treatments for 2c–3e bonds is still under debate ([17] and references therein). Usually, the bond lengths and the binding energies are overestimated within the DFT methods but on a set of small radicals we obtained similar values for these properties with BH&HLYP as with CCSD(T) calculations [20]. Moreover, in his study on the characterization of the 2c–3e bonding based on appropriate localized molecular orbital, Maity showed that molecular properties obtained with BH&HLYP/6-31++G(d,p) and MP2/6-31++G(d,p) were in good agreement [21]. We thus privileged the BH&HLYP functional in the spin-unrestricted formalism and used the standard 6-31G(d) basis set. The use of this relatively small basis set is justified by the fact that DFT methods are not very basis-set dependent. All structures were fully optimised using the analytical gradient technique, and the nature of each located stationary point was checked by evaluating harmonic frequencies. Time-dependent density functional theory with BH&HLYP/cc-pVTZ was used to calculate the UV–Visible transitions of the S.·.X^+ bonds. All these structural and energy calculations were performed with the Gaussian03 package [22]. However, to test the validity of TD-DFT results, the accurate but very expensive MRCI+Q method (see Supplementary material) was also employed with the cc-pVTZ basis set for one complex. The corresponding calculations were performed using the Molpro package [23]. The topological analyses of the AIM and ELF functions were carried out with the Topmod program [24,25], developed in the Laboratoire de Chimie Théorique and visualized with the Molekel 4.3 software [26].

4. Results and discussion

We considered radical cations resulting from the interaction between dimethylsulphide cation $(Me)_2S^+$ (Me = CH_3) and various compounds (dimethylsulphide Me_2S, amino methane NH_2Me, acetic acid MeCOOH, and the amides MeNHCOH and $MeCONH_2$. Three kinds of starting structures were built: (i) both fragments of the complex were oriented in such a way that they could form a S.·.X bond with an optimum overlap of the orbitals and the radical cation obtained was fully optimised (these results are noted (a) in Tables 1–3). (ii) For three of the radical cations (the S.·.S one and those with the O or N of the peptidic group) the fragments were oriented to mimic the constraints resulting of the environment in radical cations of some conformations of the dipeptides Met Gly, Gly Met or Met Met. (iii) Finally, we built three intermediate structures in which the fragments were in the optimised orientation of (i) but with the S.·.X distances of the constrained structures (ii). Single point calculations were performed for the (ii) and (iii) structures and are respectively noted as (c) and (b) in Tables 1–3. Our aim was to test the influence of the SX distance (comparison between (a) and (b)) and of the fragment orientations (comparison between (b) and (c)) on energies, absorption wavelengths, structural and topological parameters.

4.1. Energies and geometries

The optimised and the constrained structures of these complexes are shown in Fig. 1. Table 1 gives the absolute energies, the bond dissociation energies (BDE) of the optimised structures, the bond dissociation enthalpies $\Delta H(0\,K)$, and the SX distances. Varying the X atom and the substituents leads to changes in the energies and geometries of the optimised structures. First, due to the hindrance of the S atom, the S.·.S bond is always longer than the other S.·.X bonds. As for the S.·.N bonds, going from an amine to an amide function increases the bond length of 0.15 Å (from 2.52 to 2.77). Moreover when successive substitutions of the hydrogen atoms of the amino methane by methyl groups are performed, the S.·.N distance remains first quasi-constant (2.52 Å for $-NH_2Me$ and 2.54 Å for $-NHMe_2$) and finally increases up to 2.66 Å (for $-NMe_3$). Furthermore, replacement of the amine $-NHMe_2$ by an amide $-MeCONH_2$ enhances this lengthening, probably because of electronic factors. The S.·.O bond is shorter by 0.1 Å with the amide than with the carboxylic group. It is interesting to notice that when $(Me)_2S^+$ is in interaction with an amide function, either by bonding with N or with O, the radical cation is more stable with a S.·.O bond than with a S.·.N one by 2 kcal mol^{-1}. The geometry results obtained on S.·.N^+ and S.·.O^+ compounds can be compared to those of Brunelle and Rauk [9], although they used B3LYP/6-31G(d), which is known to generally overestimate 2c–3e bond lengths [27]. For Me_2S.·.NH_2Me^+ (named **2h** in their paper) we found a shorter SN distance than theirs (2.52 Å against 2.61 Å). Conversely the SO distances are quasi-equal in the compounds with amide groups (2.44 Å for Me_2S.·.$OC(H)NHMe^+$ (**2d**) and 2.46 Å for Me_2S.·.$OC(H)NH_2^+$ (**2c**), 2.41 Å in our work for Me_2S.·.$OCMeNH_2^+$). The SS distance in Me_2S.·.SMe_2^+ (2.84 Å) is in good agreement with the MP2/6-31+G(d) one (2.79 Å) ([28] and references therein).

The range of the BDE values (70–120 kJ mol^{-1}) corresponds to that of typical (2c–3e) bonded radical cations [21]. For $Me_2SSMe_2^+$, our result is in agreement with the one obtained with the MP2 method [28] (128.7 kJ mol^{-1}). The $\Delta H(0)$ value of $Me_2SNH_2Me^+$ is very close to the one found with the CBS-RAD method [9] (104.0 kJ mol^{-1}). These quantities strongly depend on the substituents: thus a decrease of 60 kJ mol^{-1} occurs after the substitution of H by COH in $Me_2SNH_2Me^+$ and an increase of 40 kJ mol^{-1} after substitution of OH by NH_2 in $Me_2SOCMeNH_2^+$, consistently with the variations of the SX bond distances.

As it could be expected the optimised structures are the most stable, however, the stabilisation is weak compared to the intermediate ones (b) (by 1.3 kJ mol^{-1} for S.·.S, 4.2 kJ mol^{-1} for S.·.N and quasi-equal for S.·.O containing compounds). The energies of the constrained structures (c) are higher (by 29.3 kJ mol^{-1} for S.·.S, 92.0 kJ mol^{-1} for S.·.N and 87.8 kJ mol^{-1} for S.·.O containing radicals). The angles CSX are always close to 90° in optimised structures (a), characteristic of the involvement of the 3p orbital of S (Fig. 1). They are modified in constrained structures (c). For

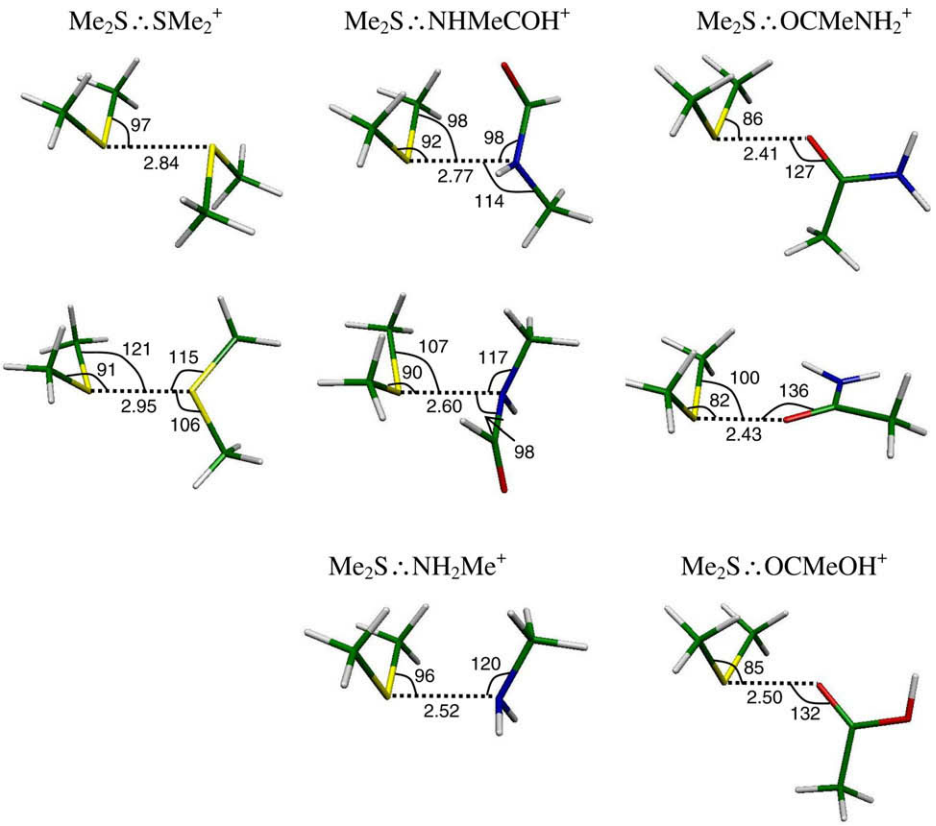

Fig. 1. Representative BH&HLYP/6-31G(d) structures of the radical cations. For the models built with SMe_2, and the amide $MeCONH_2$ (either with N or O) the first line correspond to optimised structures, whereas, the second one corresponds to constrained structures. For the models built with NH_2Me and MeCOOH only optimised structures were considered. Distances are in Å and angles in degrees.

Table 1
Absolute energies E (a.u.), S–X distances (Å), bond dissociation energies BDE and enthalpies $\Delta H(0K)$ (kJ.mol^{-1}), and spectroscopic properties: absorption wavelengths λ (nm), oscillator strengths f and the associated weighting coefficient of the dominant transition in parentheses. (a) Optimised, (b) intermediate and (c) constrained structures. All spectroscopic properties were calculated with the TD-DFT method(BH&HLYP/cc-pVTZ) except those with an asterisk, calculated with MRCI+Q/cc-pVTZ.

Model	E	d(S–X)	BDE	$\Delta H(0\,K)$	λ	f
$Me_2S{\cdot}{\cdot}SMe_2^+$ (a)	−955.60348	2.84	119.5	115.8	460	0.28 $\sigma_{SS}\rightarrow\sigma^*_{SS}$ (0.98)
$Me_2S{\cdot}{\cdot}SMe_2^+$ (b)	−955.60300	2.95			523	0.29 $\sigma_{SS}\rightarrow\sigma^*_{SS}$ (0.98)
$Me2S{\cdot}{\cdot}SMe_2^+$ (c)	−955.59236	2.95			596	0.27 $\sigma_{SS}\rightarrow\sigma^*_{SS}$ (0.97)
$Me_2S{\cdot}{\cdot}NH_2Me^+$ (a)	−573.45693	2.52	123.3	112.9	365	0.26 $\sigma_{SN}\rightarrow\sigma^*_{SN}$ (0.97)
$Me_2S{\cdot}{\cdot}NHMeCOH^+$ (a)	−686.72228	2.77	66.9	62.2	531 471*	0.15 $\sigma_{SN}\rightarrow\sigma^*_{SN}$ (0.99)
$Me_2S{\cdot}{\cdot}NHMeCOH^+$ (b)	−686.72074	2.60			456	0.14 $\sigma_{SN}\rightarrow\sigma^*_{SN}$ (0.97)
$Me_2S{\cdot}{\cdot}NHMeCOH^+$ (c)	−686.68713	2.60			481 422*	0.19 $\sigma_{SN}\rightarrow\sigma^*_{SN}$ (0.99)
$Me_2S{\cdot}{\cdot}OCMeOH^+$ (a)	−706.61213	2.50	86.9	80.2	339	0.09 $\sigma_{SO}\rightarrow\sigma^*_{SO}$ (0.73)
$Me_2S{\cdot}{\cdot}OCMeNH_2^+$ (a)	−686.76079	2.41	128.3	125.9	387	0.17 $\sigma_{SO}\rightarrow\sigma^*_{SO}$ (0.95)
$Me_2S{\cdot}{\cdot}OCMeNH_2^+$ (b)	−686.76075	2.43			395	0.18 $\sigma_{SO}\rightarrow\sigma^*_{SO}$ (0.95)
$Me_2S{\cdot}{\cdot}OCMeNH_2^+$ (c)	−686.72732	2.43			412	0.20 $\sigma_{SO}\rightarrow\sigma^*_{SO}$ (0.98)

The BDE's and the $\Delta H(0\,K)$'s are associated to the following dissociation reaction: $(Me)_2S{\cdot}{\cdot}Y^+ \rightarrow (Me)_2S^+ + Y$.

instance in $Me_2S{\cdot}{\cdot}SMe_2^+$ three of the $\angle CSS$ angles increase from 97° in the optimised structure to a maximum value of 121° in the constrained one. Moreover there is a torsion around the SS bond (the smallest $\angle CSSC$ dihedral angles vary from 78° to 135°). Thus it appears that the major factor of destabilisation is the orientation of the fragments.

Table 2
AIM topological parameters of the investigated models (X = N,O, S): S.·.X bond critical point (BCP) properties (R_s, ρ, $\nabla^2\rho$)[a], integrated spin densities, $\langle S_z\rangle$, in the atomic basins S or X, as well as the delocalization index $\delta_{S,X}$ between these basins for (a) the optimised structures, (b) the intermediate structures and (c) the constrained structures.

Model	R_S	ρ	$\nabla^2\rho$	$\langle S_z\rangle_S$	$\langle S_z\rangle_X$	$\delta_{S,X}$
$Me_2S.\cdot.SMe_2^+$ (a)	1.42	0.037	0.064	0.24	0.24	0.54
$Me_2S.\cdot.SMe_2^+$ (b)	1.48	0.031	0.055	0.24	0.24	0.50
$Me_2S.\cdot.SMe_2^+$ (c)	1.44	0.029	0.060	0.23	0.23	0.52
$Me_2S.\cdot.NH_2Me^+$ (a)	1.45	0.028	0.060	0.30	0.17	0.52
$Me_2S.\cdot.NHMeCOH^+$ (a)	1.46	0.037	0.083	0.35	0.10	0.32
$Me_2S.\cdot.NHMeCOH^+$ (b)	1.37	0.038	0.082	0.34	0.11	0.38
$Me_2S.\cdot.NHMeCOH^+$ (c)	1.32	0.045	0.093	0.31	0.15	0.44
$Me_2S.\cdot.OCMeOH^+$ (a)	1.26	0.044	0.119	0.40	0.07	0.30
$Me_2S.\cdot.OCMeNH_2^+$ (a)	1.28	0.042	0.114	0.37	0.11	0.40
$Me_2S.\cdot.OCMeNH_2^+$ (b)	1.28	0.042	0.118	0.37	0.10	0.40
$Me_2S.\cdot.OCMeNH_2^+$ (c)	1.31	0.035	0.101	0.37	0.10	0.40

[a] R_S = distance between atom S and the bond critical point; ρ is the electronic density at the BCP and $\nabla^2\rho$ the laplacian of ρ at this point.

Table 3
ELF topological parameters of the investigated models (X = N, O and S): integrated spin densities, $\langle S_z\rangle$, in the monosynaptic basins V(S) or V(X), delocalization index $\delta_{V(S),V(X)}$ between these basins, as well as 2c–3e bifurcation index θ(3e) for (a) the optimised structures, (b) the intermediate structures and (c) the constrained structures. V(O) represents the union of the two monosynaptic basins of O.

Model	$\langle S_z\rangle_{V(S)}$	$\langle S_z\rangle_{V(X)}$	$\delta_{V(S),V(X)}$	θ(3e)
$Me_2S.\cdot.SMe_2^+$ (a)	0.18	0.18	0.38	0.09
$Me_2S.\cdot.SMe_2^+$ (b)	0.18	0.18	0.38	0.05
$Me_2S.\cdot.SMe_2^+$ (c)	0.18	0.18	0.38	0.01
$Me_2S.\cdot.NH_2Me^+$ (a)	0.23	0.09	0.28	0.09
$Me_2S.\cdot.NHMeCOH^+$ (a)	0.26	0.04	0.16	−0.02
$Me_2S.\cdot.NHMeCOH^+$ (b)	0.26	0.05	0.18	0.02
$Me_2S.\cdot.NHMeCOH^+$ (c)	0.23	0.07	0.22	0.05
$Me_2S.\cdot.OCMeOH^+$ (a)	0.29	0.06	0.18	−0.06
$Me_2S.\cdot.OCMeNH_2^+$ (a)	0.27	0.09	0.28	0.00
$Me_2S.\cdot.OCMeNH_2^+$ (b)	0.27	0.09	0.26	−0.01
$Me_2S.\cdot.OCMeNH_2^+$ (c)	0.27	0.08	0.28	−0.01

4.2. Topological analysis

The nature of the S.·.X bond was investigated by AIM (Table 2) and ELF (Fig. 2 and Table 3) topological analyses. Table 2 shows that the first AIM signature of the 2c–3e bond is verified, i.e. at the bond critical point the electronic density is low and its laplacian is positive.

The ELF topology of all the radicals is in accordance with the qualitative signature of a 2c–3e bond, as illustrated in Fig. 2 for three representative systems, i.e. absence of disynaptic basin V(S,X), for X = S, N and O. Furthermore, we have verified that the two monosynaptic basins V(S) and V(X) share a common separatrix.

4.2.1. Optimised structures (a)

Table 2 shows that, as expected, the lone electron is shared between the S and X atoms (since the sum of the atomic integrated spin densities is quasi-equal to 0.5, the total spin of the radical). Table 3 specifies this localization, which arises mostly in the monosynaptic basins of the two heteroatoms (the sum of the $\langle S_z\rangle_{V(S)}$ and $\langle S_z\rangle_{V(X)}$ values is lower than 0.5 because the neighbouring core and valence basins also contribute to the spin density). This was expected from the Pauling description on the 2c–3e bonds in terms of resonating Lewis structures. Obviously if X = S the integrated spin density $\langle S_z\rangle$ is equally shared between the two atoms (Table 2) or between the two V(S) basins (Table 3). For X = N, the spin is mainly localized on S (respectively on the V(S) basin). Moreover the bond is more spin polarized if S is bonded to N of a peptidic bond than with N of an amino group. The spin localization on S is even more enhanced for X = O, in agreement with the increase of the difference in atom electronegativities. The 2 $\langle S_z\rangle_X$ values arising from our AIM analysis can be compared to the Mulliken description of the spin distribution that was used by Brunelle and Rauk [9]. For $Me_2S.\cdot.NH_2Me^+$ (**2h**) they found that 59% of the spin is on S and 39% is localized on N which is in excellent agreement with our values (60% on S and 34% on N). For the compounds with amide groups, they obtained 71% on S and 27% on O for $Me_2S.\cdot.OC(H)NHMe^+$ (**2d**) and 73% on S and 25% on O for $Me_2S.\cdot.OC(H)NH_2$ (**2c**), which still compares very well with our results on $Me_2.\cdot.OCMeNH_2^+$ (74% for S and 22% for O).

The delocalization δ of the electronic density between the S and X atomic basins (respectively between the V(S) and V(X) basins) decreases as the difference in spin polarization between S and X (respectively between V(S) and V(X)) increases, i.e. roughly in the series S, N, O, as shown by the last column of Table 2 (respectively the third column of Table 3). Finally the core valence bifurcation (CVB) index θ(3e) arising from the ELF analysis (see Table 3) is positive for the optimised $Me_2S.\cdot.SMe_2^+$ and $Me_2S.\cdot.NH_2Me^+$ (respectively negative or null for the others models). Actually the sign of θ(3e) is closely related to the difference in spin polarization and to the magnitude of δ: it is negative if the spin is mainly localized on S and the delocalization index is low. As a conclusion, among the five optimised models, only $Me_2S.\cdot.SMe_2^+$ and $Me_2S.\cdot.NH_2Me^+$ fulfill the four topological criteria and can be considered as 2c–3e compounds, whereas, in the three remaining ones the S.·.X bonds are mainly of electrostatic nature. For the two models with X = O, this result is in agreement with our preceding paper dealing with the characterization of the S.·.O bond in anion, neutral and cation radicals [20].

4.2.2. Intermediate and constrained structures

It is worth investigating the variations of the quantitative topological signatures (i) as the SX distance varies (from (a) to (b) structures) and (ii) as the relative orientation of the fragments varies (from (b) to (c) structures).

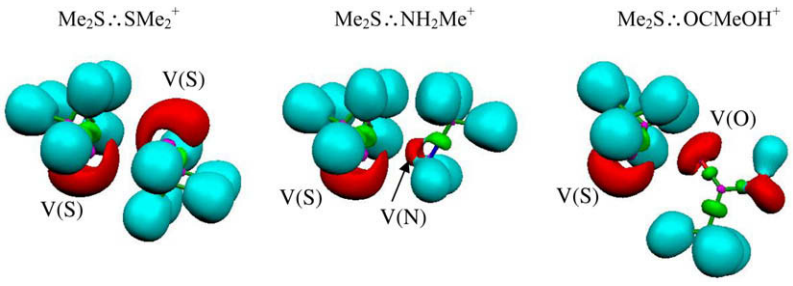

Fig. 2. ELF = 0.8 isosurface of three representative radical cations. The name of the monosynaptic basins involved in the S.·.X^+ bonds are indicated.

(i) The spin distribution is quasi-unchanged as the SX distance increases (in $Me_2S^{\cdot}\therefore SMe_2^+$) or decreases ($Me_2S^{\cdot}\therefore NHMeCOH^+$) (Tables 1–3). On the other hand the delocalization index δ_{SX} between the S and X (X = S or N) atomic basins decreases as the SX distance increases (for $Me_2S^{\cdot}\therefore NHMeCOH^+$, the SN distance varies from 2.60 to 2.77 Å and δ_{SN} from 0.44 to 0.38, Table 2). This trend is smoothed when considering $\delta_{V(S),V(X)}$ because the integrated electron density is lower in the monosynaptic basins (ELF) than in the atomic ones (AIM) (for $Me_2S^{\cdot}\therefore NHMeCOH^+$ $\delta_{V(S),V(N)}$ varies from 0.22 to 0.18). As for the CVB index, it is related to the variations of the SX distances: indeed for $Me_2S^{\cdot}\therefore SMe_2^+$ it decreases from 0.09 to 0.05 by a 0.11 Å increase of the SS bond length. For $Me_2S^{\cdot}\therefore NHMeCOH^+$ it becomes positive (from −0.02 to 0.02) by a 0.17 Å decrease of the SN distance. For $Me_2S^{\cdot}\therefore OCMeNH_2^+$ the change is negligible, because the SO distance does not vary.

(ii) As the fragments are reoriented the spin distribution and consequently the delocalization indexes vary noticeably only for $Me_2S^{\cdot}\therefore NHMeCOH^+$: the delocalization index increases because of the spin transfer from S to N. The CVB is sensitive to the orientations for $S^{\cdot}\therefore S^+$ and $S^{\cdot}\therefore N^+$ models: indeed it decreases from 0.05 to 0.01 for $Me_2S^{\cdot}\therefore SMe_2^+$ and increases from 0.02 to 0.05 for $Me_2S^{\cdot}\therefore NHMeCOH^+$. Surprisingly no variation is observed for the $S^{\cdot}\therefore O^+$ models despite the important reorientation of the fragments.

In conclusion, the distance and orientation variations lead to major effects on the 2c–3e character of the $S^{\cdot}\therefore X$ bonds: a lowering for the $S^{\cdot}\therefore S$ radicals and an enhancement for the $S^{\cdot}\therefore N$ ones, whereas, the $S^{\cdot}\therefore O$ bond remains mostly of electrostatic nature. These trends could be used to predict the nature of the $S^{\cdot}\therefore X$ bond in a constrained environment, like in polypeptides.

4.3. Spectroscopy

The absorption wavelengths and the oscillator strengths of the most intense transitions obtained by TD-DFT are reported in Table 1. The transitions are mainly $\sigma_{sx} \rightarrow \sigma^*_{SX}$ as shown by the weighting coefficients (Table 1). They are either in the near-UV region or in the visible. The wavelengths strongly vary not only with the nature of X, but also with the geometries.

For the $S^{\cdot}\therefore O$ bond with the carboxylic group and $S^{\cdot}\therefore N$ bond with the amine function, the transitions are in the near-UV region, the lowest wavelengths being found with the carboxylic function (339 nm) and with the amine one (365 nm). The wavelengths are in the visible region if N or O comes from an amide group. A bathochromic effect is observed by increasing the SX distances (structures (a) and (b)). This corresponds to a decrease of the $\sigma_{SX}/\sigma^*_{SX}$ separation due to a decrease of the associated S and X lone pairs orbitals overlap. The relative orientations of both fragments are also important as shown by the comparison between the optical properties of intermediate (b) and constrained (c) structures (λ increases in the three investigated cases). Indeed, we have verified that because of changes in the valence and dihedral angles the alignment of the lone pair orbitals is somehow damaged and thus the overlap of the lone pairs decreases. By combining both effects, the bathochromic effect is especially large for the $S^{\cdot}\therefore S^+$ radicals, the wavelength increases from 460 nm in the optimised structure (a) to 596 nm in the constrained one (c). Indeed the SS bond is elongated by only 0.11 Å but the valence (Fig. 1) and dihedral angles are strongly modified (*vide supra*). The wavelength change is less important for $Me_2S^{\cdot}\therefore NHMeCOH^+$ (from 531 nm to 481 nm) associated with a shortening of 0.17 Å and smaller angle variations. As for $Me_2S^{\cdot}\therefore OCMeNH_2^+$ the SO distance is quasi-constant, thus the slight wavelength change (390–410 nm) comes from orientation variations (Fig. 1). The oscillator strengths are of the same magnitude and relatively high (in a range of 0.15–0.28), except for $Me_2S^{\cdot}\therefore OCMeOH^+$ (0.09). Conversely to the absorption wavelengths, they are quasi-insensitive to geometry variations (from (a) to (c) structures). They remain close to 0.28 for $Me_2S^{\cdot}\therefore SMe_2^+$ radicals and to 0.18 for $Me_2S^{\cdot}\therefore OCMeNH_2^+$ ones. The variation is more important for $Me_2S^{\cdot}\therefore NHMeCOH^+$, from 0.14 in the intermediate structure to 0.19 in the constrained one.

For this latter complex, we have performed MRCI+Q calculations (Table 1) for the optimised (a) and constrained (c) structures. The wavelength is lowered by about 60 nm from TD-BH&HLYP to MRCI+Q method, whatever the structure. This corresponds to an energy gap of less than 0.5 eV (0.30 eV for (a) and 0.36 eV for (b)) which is the maximum error reported for the TD-DFT method [29]. However, the evolutions between (c) and (a) structures are similar: we observe the same hypsochromic effect of ca. 50 nm in both cases. Nevertheless, the MRCI+Q method can hardly be used for larger systems, being too much time and memory-consuming. Hence the TD-DFT calculations can remain a good compromise, keeping in mind the limits of validity of their results.

Furthermore, these results are in good agreement with the values obtained in other theoretical spectroscopic studies concerning similar compounds. These properties were computed for several $S^{\cdot}\therefore X^+$ cations using TD-B3LYP/6-311+G(d,p) [8,10], TD-B3LYP/6-311++G(d,p) [30] or semi empirical methods [10]. In most of radicals involving amides the SO distance remains remarkably constant around 2.4 Å, and the wavelengths are around 390 nm, close to our values of 390–410 nm in $Me_2S^{\cdot}\therefore OCMeNH_2^+$. For solvated *N*-acetylmethionineamide, Brunelle et al. have studied the influence of the bond distance on the absorption wavelength to fit the observed spectrum. They found λ values of 480 nm for the optimised SN distance of 2.7 Å and 440 nm for 2.6 Å [8]. Our results are in qualitative agreement: for Me_2 $S^{\cdot}\therefore NHMeCOH^+$ the distance varies from 2.77 (optimised) to 2.60 Å (constrained) and λ from 531 to 481 nm.

5. Conclusion

The aim of this work was to reinvestigate the nature of $S^{\cdot}\therefore X$ bonds formed by interaction of sulphur radical cation with groups containing heteroatoms S, N or O. The formation of such bonds after one-electron oxidation of peptides, proteins or organic compounds has been documented experimentally. However, since these transients have very short lifetime (usually in the tens of microsecond timescale), their identification remains difficult and is based on absorption spectra. Energy considerations indicate that in the studied models, some constraints, like those that can exist in peptides or proteins, destabilize the sulphur radical cation. Whereas, the SX bond length variation does not affect much its stability, the orientation can have a relatively high effect. The topological analysis shows that the nature of the 2c–3e bond in $S^{\cdot}\therefore X^+$ radicals varies with X, from a purely 2c–3e bond in $S^{\cdot}\therefore S^+$ entities to electrostatic interaction in $S^{\cdot}\therefore O^+$ ones. As for $S^{\cdot}\therefore N^+$ radicals, their nature depends on the nitrogen function (peptidic or amine) and on the geometrical constraints.

There are no experimental values for the absorption spectra of the small models studied here, however, on the basis of experimental data obtained on larger molecules or on peptides, absorption wavelengths were attributed to the various $S^{\cdot}\therefore X^+$ radicals [6,12]. Theoretical determinations (ours as well as those already published in the literature [8–11]) confirm that $S^{\cdot}\therefore O^+$ radical spectra should peak around 400 nm. However, in agreement with preceding works, we show that the absorption maxima of the other radicals can vary with the local geometry. For instance, using TD-DFT, the values obtained on our constrained radicals reproduc-

ing some peptidic environment indicate that the $S_{\cdot}.S^{+}$ radical might absorb around 600 nm and the $S_{\cdot}.N^{+}$ one around 480 nm. Caution should thus be taken when determining the nature of the X atom involved in $S_{\cdot}.X^{+}$ radicals. Finally the different characterisations of the short-lived species reported in this work (structural, topological and spectroscopic) might provide clues to predict some reactivity of methionine residues in proteins.

Acknowledgement

We thank IDRIS for computer time (Project 070268).

Appendix A. Supplementary material

Supplementary data associated with this article can be found, in the online version, at doi:10.1016/j.cplett.2008.11.012.

References

[1] W. Vogt, Free Radic. Biol. Med. 18 (1995) 93.
[2] R.L. Levine, B.S. Berlett, J. Moskovitz, L. Mosoni, E.R. Stadtman, Mech. Age. Dev. 107 (1999) 323.
[3] A.D. Butterfield, Chem. Res. Toxicol. 10 (1997) 495.
[4] I. Dalle-Donne, R. Rossi, D. Giustarini, N. Gagliano, P. Di Simplicio, R. Colombo, A. Milzani, Free Radic. Biol. Med. 32 (2002) 927.
[5] T. Clark, Sulphur-centered reactive intermediates in: C. Chatgilialoglu, D. Asmus (Eds.), Chemistry and Biology, NATO-ASI Studies, Plenum Press, New York, 1990, p. 13 (197).
[6] K.D. Asmus, Present status and future trends, in: C.D. Jonah, B.S.M. Rao (Eds.), Radiation Chemistry, Elsevier, Amsterdam, 2001, p. 341.
[7] K. Bobrowski, C. Houée-Levin, B. Marciniak, Chimia 62 (2008) 728.
[8] P. Brunelle, C. Schöneich, A. Rauk, Can. J. Chem. 84 (2006) 893.
[9] P. Brunelle, A. Rauk, J. Phys. Chem. A 108 (2004) 11032.
[10] D. Pogocki, C. Schöneich, J. Org. Chem. 67 (2002) 1526.
[11] D. Pogocki, K. Serdiuk, C. Schöneich, J. Phys. Chem. A 107 (2003) 7032.
[12] G.L. Hug, K. Bobrowski, D. Pogocki, G. Hörner, B. Marciniak, Chem. Phys. Chem. 8 (2007) 2202.
[13] L. Pauling, J. Am. Chem. Soc. 53 (1931) 3225.
[14] R.F.W. Bader, Atoms in Molecules: A Quantum Theory, Oxford University Press, Oxford, UK, 1990.
[15] A.D. Becke, K.E. Edgecombe, J. Chem. Phys. 92 (1990) 5397.
[16] B. Silvi, A. Savin, Nature 371 (1994) 683.
[17] I. Fourré, B. Silvi, Heteroat. Chem. 18 (2007) 135.
[18] J. Bergès, F. Fuster, J.-P. Jacquot, B. Silvi, C. Houée-Levin, Nukleonika 45 (2000) 23.
[19] I. Fourré, B. Silvi, A. Sevin, H. Chevreau, J. Phys. Chem. A 106 (2002) 2561.
[20] I. Fourré, J. Bergès, J. Phys. Chem. A 108 (2004) 898.
[21] D.K. Maity, J. Phys. Chem. A 106 (2002) 5716.
[22] M.J. Frisch, Gaussian 03, Revision C.02, Gaussian, Inc., Wallingford CT, 2004.
[23] H.-J. Werner et al., Molpro, version 2006.1, A Package of Ab initio Programs, see http://www.molpro.net.
[24] S. Noury, X. Krokidis, F. Fuster, B. Silvi, Topmod Package (1997).
[25] S. Noury, X. Krokidis, F. Fuster, B. Silvi, Comput. Chem. 23 (1999) 597.
[26] P. Flükiger, H.P. Lüthi, S. Portmann, J. Weber, Molekel 4.3; Swiss National Supercomputing Centre CSCS, Manno (Switzerland), 2000.
[27] B. Braïda, P. Hiberty, A. Savin, J. Phys. Chem. A 102 (1998) 7872.
[28] J. Bergès, N. Varmenot, A. Scemama, Z. Abedinzadeh, K. Bobrowski, J. Phys. Chem. A 112 (2008) 7015.
[29] A. Dreuw, M. Head-Gordon, Chem. Rev. (2005) 4009.
[30] K. Bobrowski, G.L. Hug, D. Pogocki, B. Marciniak, C.J. Schöneich, Am. Chem. Soc. 129 (2007) 9236.